Article

Reprogramming yeast metabolism for customized starch-rich micro-grain through low-carbon microbial manufacturing

Zhihui Shi [1,2,3,4,5,6], Zhaoyu Xu[1,4,6], Weihe Rong[1,3,4,5], Hongbing Sun[1,3,4], Hongyi Zhou[1,2,3,4,5], Qianqian Yuan [1,3,4], Aixuan Xiao[1,3,4,5], Hongfei Ma[1,3,4,5], Tao Cai [1,3,4] ✉, Guokun Wang [1,3,4,5] ✉ & Yanhe Ma [1,4] ✉

Starch is a primary food ingredient and industrial feedstock. Low-carbon microbial manufacturing offers a carbon-neutral/negative arable land-independent strategy for starch production. Here, we reconfigure the oleaginous yeast as a starch-rich micro-grain producer by rewiring the starch biosynthesis and gluconeogenesis pathways and regulating cell morphology. With the CO_2 electro-synthesized acetate as the substrate, the strain accumulates starch 47.18% of dry cell weight. The optimized system renders spatial-temporal starch productivity (243.7 g/m²/d) approximately 50-fold higher than crop cultivation and volumetric productivity (160.83 mg/L/h) over other microbial systems by an order of magnitude. We demonstrate tunable starch composition and starch-protein ratios via strain and process engineering. The engineered artificial strains adopt a cellular resources reallocation strategy to ensure high-level starch production in micro-grain and could facilitate a highly efficient straw/cellulose-to-starch conversion. This work elucidates starch biosynthesis machinery and establishes a superior-to-nature platform for customizable starch synthesis, advancing low-carbon nutritional manufacturing.

Starch is an essential food ingredient and energy source to meet humans' nutritional requirements[1]. The annual global demand for starch is above 120 million tons and is projected to grow at a compound annual growth rate of 4–5% as a result of population growth, consumption upgrading, as well as increasing starch demand in industrial applications[2,3]. Starch supply through the current production mode, traditional agriculture/crop cultivation, can barely meet the dramatically growing demand due to (i) the limited arable land[4,5], (ii) the rate constraint of natural photosynthesis-based carbon fixation[6], and (iii) the threat of climate change such as CO_2 emission and global warming[7].

CO_2-to-starch conversion through low-carbon biomanufacturing is a possible approach to address the challenges and reshape a carbon-negative food supply route via cellular agriculture[8,9]. With the consumption of renewable electricity, CO_2 was electro-catalyzed to liquid energy-rich C1/C2 chemicals, such as formate and acetate[10]. These short-chain substrates are then transformed into more complex compounds by enzymatic catalysis[11] or microbial transformation[12,13]. The whole process enables an energy efficiency four-fold higher than natural photosynthesis, representing an energy-efficient approach for food ingredient production[14].

In the past several years, there have been continuous breakthroughs in CO_2 electro-conversion to ensure the production of pure

[1]Tianjin Institute of Industrial Biotechnology, Chinese Academy of Sciences, Tianjin 300308, China. [2]University of Chinese Academy of Sciences, Beijing 100049, China. [3]State Key Laboratory of Engineering Biology for Low-Carbon Manufacturing, Tianjin 300308, China. [4]National Center of Technology Innovation for Synthetic Biology, Tianjin 300308, China. [5]TIB-UM Joint Laboratory of Synthetic Biology for Traditional Chinese Medicine, Tianjin 300308, China. [6]These authors contributed equally: Zhihui Shi, Zhaoyu Xu. ✉e-mail: cai_t@tib.cas.cn; wanggk@tib.cas.cn; ma_yh@tib.cas.cn

acetate at a CO_2 fixation rate dramatically higher than natural photosynthesis[12,15]. The subsequent conversion of acetate to starch, however, demands microbes capable of synthesizing and accumulating starch at a superior-to-nature rate and content. The food-safe yeast *Yarrowia lipolytica* strain[16], which could naturally assimilate acetate[17] and produce a variety of health-relevant molecules at high levels[18–20], is an excellent chassis strain to develop as an efficient producer of starch-rich micro-grain.

Herein, we reconfigure the oleaginous yeast to an efficient work-house for starch biosynthesis by rewiring the starch biosynthesis and gluconeogenesis pathways, and regulating cell morphology (Fig. 1). The engineered strains lay the foundation to understand the natural and remodeled machinery for starch biosynthesis, and facilitate a superior-to-nature high-level production of starch with customized composition.

Results

Improving starch production by implementation of heterologous starch biosynthesis pathway

Yeast *Y. lipolytica* strain can naturally accumulate starch/glycogen due to the presence of UTP-glucose-1-phosphate uridylyltransferase and glycogen synthase enzymes converting glucose-1-phosphate to (G1P) to amylose via UDP-glucose (Fig. 2a). The starch production of the wild-type strain was, however, very low when the strain assimilated acetate as the sole carbon source (up to 30.48 mg/L/OD$_{600}$, Fig. 2b). To improve the strain's capacity for starch production, we introduced heterologous starch biosynthesis pathway (SBP) consisting of glucose-1-phosphate adenylyltransferase and starch synthase (Fig. 2a) driven by the strong GPD and TEF promoters under acetate condition, which were selected through RNAseq-guided identification and validation (Supplementary Table 1 and Supplementary Fig. 1). The engineered strain ST503

implemented with SBP from *Cereibacter sphaeroides* accumulated starch at a significantly higher level- up to 133.08 mg/L/OD$_{600}$ (Fig. 2c). Based on the cell growth and starch content profiles (Fig. 2b, c), we selected 36 h and 72 h as the optimal timepoints for the measurement of starch content during exponential and stationary phases, respectively. Engineered strains carrying SBP from *Escherichia coli* and *Synechococcus sp.* accumulated starch at various levels (Fig. 2c, d, and Supplementary Fig. 2), reaching 244.95 mg/L/OD$_{600}$ and 585.43 mg/L (the highest values of ST501 in Fig. 2d and Supplementary Fig. 2). Via an optimization of the SBP origin and expression level, we generated the ST587 strain implemented with one copy of SBP from *E. coli* and three copies of SBP from *C. sphaeroides*, showing a high starch production level up to 379.85 mg/L/OD$_{600}$ and 704.34 mg/L (Fig. 2e and Supplementary Fig. 3). Moreover, the ST587 strain grew and produced starch comparably in both commercial and electrosynthetic acetate (Fig. 2f), demonstrating the feasibility of using the synthetic *Y. lipolytica* strains for low-carbon manufacturing-based starch production.

Boosting starch accumulation by regulating the anabolism and catabolism

Starch is biosynthesized from G1P/UDP-glucose and accumulates in the cell when the carbon source is abundant, whereas, under nutrient-deficient conditions, starch is catabolized to support cell activity (Figs. 2b and 3a). An enlarged metabolic flux to G1P and abolished starch degradation would be theoretically beneficial to improve starch accumulation. To test this hypothesis, we overexpressed/deleted genes involved in gluconeogenesis and glyoxylate cycle, repressed/deleted genes for competitive diversion of G6P and UDP-glucose, and deleted genes for starch degradation, in both low- and high-level starch-producing strains, ST503 and ST587 (Fig. 3 and Supplementary Fig. 4). Single manipulation of genes in gluconeogenesis and
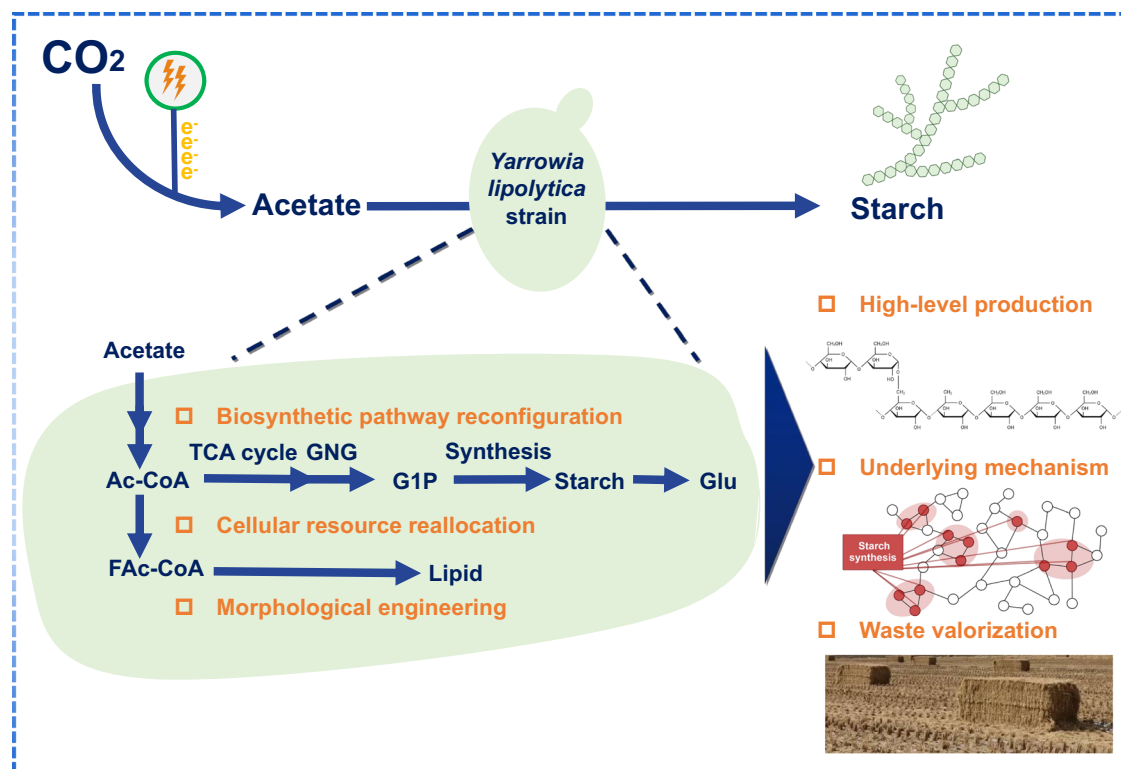

Fig. 1 | Design of an artificial yeast cell factory to facilitate the efficient starch synthesis from carbon dioxide. Acetate electro-synthesized from carbon dioxide was used as feedstock for starch synthesis by synthetic yeast *Yarrowia lipolytica*, which was systematically reprogrammed to accumulate high-level starch. The mechanism supporting the high-level starch biosynthesis was clarified, and the microbial starch production from the natural photosynthesis byproduct, straw, was demonstrated. CO_2 carbon dioxide, Ac-CoA acetyl-CoA, TCA tricarboxylic acid, GNG gluconeogenesis, Glu glucose, FAc-CoA fatty acyl-CoA. [Created in BioRender. Shi, Z. (2025) https://BioRender.com/x81f786].
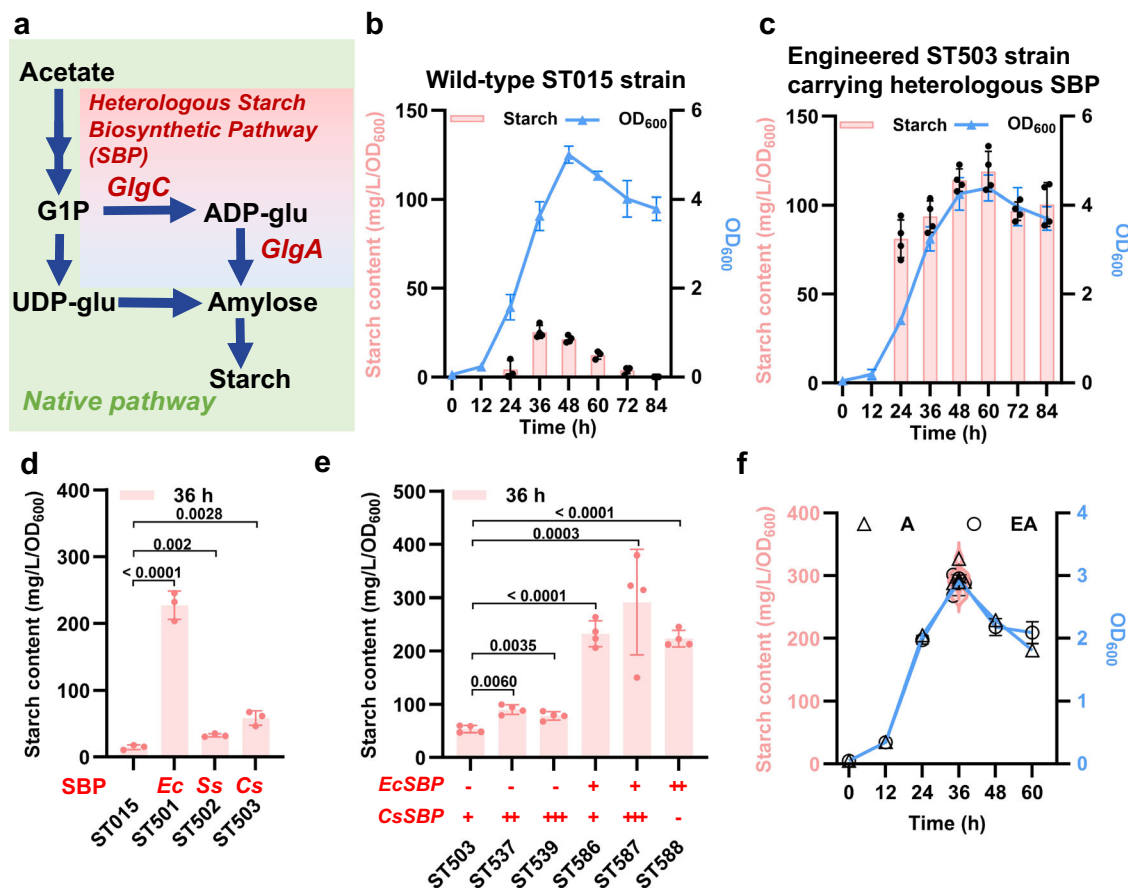
Fig. 2 | Implementation of heterologous starch biosynthesis pathway (SBP) dramatically strengthens cellular starch accumulation. a Biosynthetic pathway for starch production from acetate. G1P glucose 1-phosphate, Glu glucose. **b** and **c** Time-course cell growth and starch content of wild-type and engineered strains. **d** and **e** Starch content of engineered strains integrated SBP of various origins and/or expression levels. **f** Cell growth and starch content of ST587 cultivated with commercial acetate (A) or electrosynthetic acetic acid (EA). Strains were cultivated in 50 mL of mineral medium (MM) containing 20 g/L commercial acetate (MMA) in a shake flask (**b**, **c**) or 2.5 mL of MMA containing commercial acetate (**d**–**f**) or electrosynthetic acetic acid (**f**) in a culture tube. Data shown are mean values ± SDs of biological replicates (**b** ($n = 3$ or 4), **c** ($n = 4$), **d** ($n = 3$), **e** ($n = 4$), **f** ($n = 3$ or 4)). Starch data are presented as the median, interquartile range (IQR), and distribution of biological replicates ($n = 3$ or 4) (**f**). Statistical difference was determined by a two-tailed unpaired t-test. Source data are provided as a Source Data file.

glyoxylate cycle did not change starch production (Fig. 3b, Supplementary Fig. 4, and 5), while the combinatorial manipulation toward the enlarged flux to G1P improved starch content by 55% (ST594 vs. ST587) (Fig. 3e and Supplementary Fig. 5). Deletion of *GDB1* encoding glycogen debranching enzyme and *TPS1/TPS3* encoding trehalose 6-phosphate synthase/phosphatase in ST503 increased starch content by 22.43-73.83% (Fig. 3c, d, Supplementary Figs. 6 and 7). By deleting the glycogen debranching enzyme- and trehalose 6-phosphate synthase/phosphatase-encoding genes in ST594 to reduce starch catabolism and increase UDP-glucose supply, we generated the ST1266 strain to produce starch up to 593.99 mg/L/OD_{600} (Fig. 3f, g, Supplementary Fig. 8 and 9).

We also attempted to manipulate the energy supply system for improved starch production since a net input of 10–13 mol of ATP equivalent is required to synthesize 1 mol of starch from acetate. However, the reconstruction of an artificial ATP regeneration system through polyphosphate conversion (Supplementary Fig. 10) and formate-based NADH/ATP generation (Supplementary Fig. 11) did not further improve starch production, indicating the ATP sufficiency from the native metabolism to support a high-level starch biosynthesis.

Increasing cellular starch accumulation via cell morphology engineering

The intracellular environment is crowded, and expanding cell size may allow for a larger space for macromolecule accumulation (Fig. 4a). To test this hypothesis, we abolished the hyphae-forming ability of dimorphic *Y. lipolytica* strain by deleting the *MHY1* gene encoding a stress-responsive transcription factor (TF)[21], and verified that cells in oval shape would dramatically limit cell size and starch content (Fig. 4b, c). We then conversely attempted to stimulate hyphae formation by manipulating specific genes (Fig. 4d), including *SRG1*, *MBP1*[22], *HCP1/2*, *PFS1*, and *MHY1*[23]. Among the resulting strains, ST1269 (*SRG1* deletion), ST1271 (*MBP1* deletion), and ST1278 (overexpressing *MHY1*) notably stimulated hyphal growth (Fig. 4d), enlarged cell size, and accumulated 10.69-36.05% higher starch (up to 336.58–428.14 mg/g DCW) (Fig. 4e and Supplementary Fig. 12).

Superior-to-nature high-level production of starch with customized composition by the micro-grain

We grew three representative strains, wild-type ST015 and engineered strains ST587 (ST015 implemented with heterologous SBP pathways) and ST1271 (ST015 implemented with heterologous SBP pathways, and engineered for altered cell morphology, and remodeled anabolism and catabolism) in a mineral medium containing acetate as the sole carbon source to obtain cells containing starch, which we named micro-grain. Starch consists of non-resistant starch that can be readily digested by enzymes in the human gastrointestinal tract and resistant starch that resists digestion in the intestine and can provide dietary fiber and prebiotic benefits. The whole starch content reached the highest 290.94 and 471.82 mg/g DCW (Fig. 5a, b, Supplementary
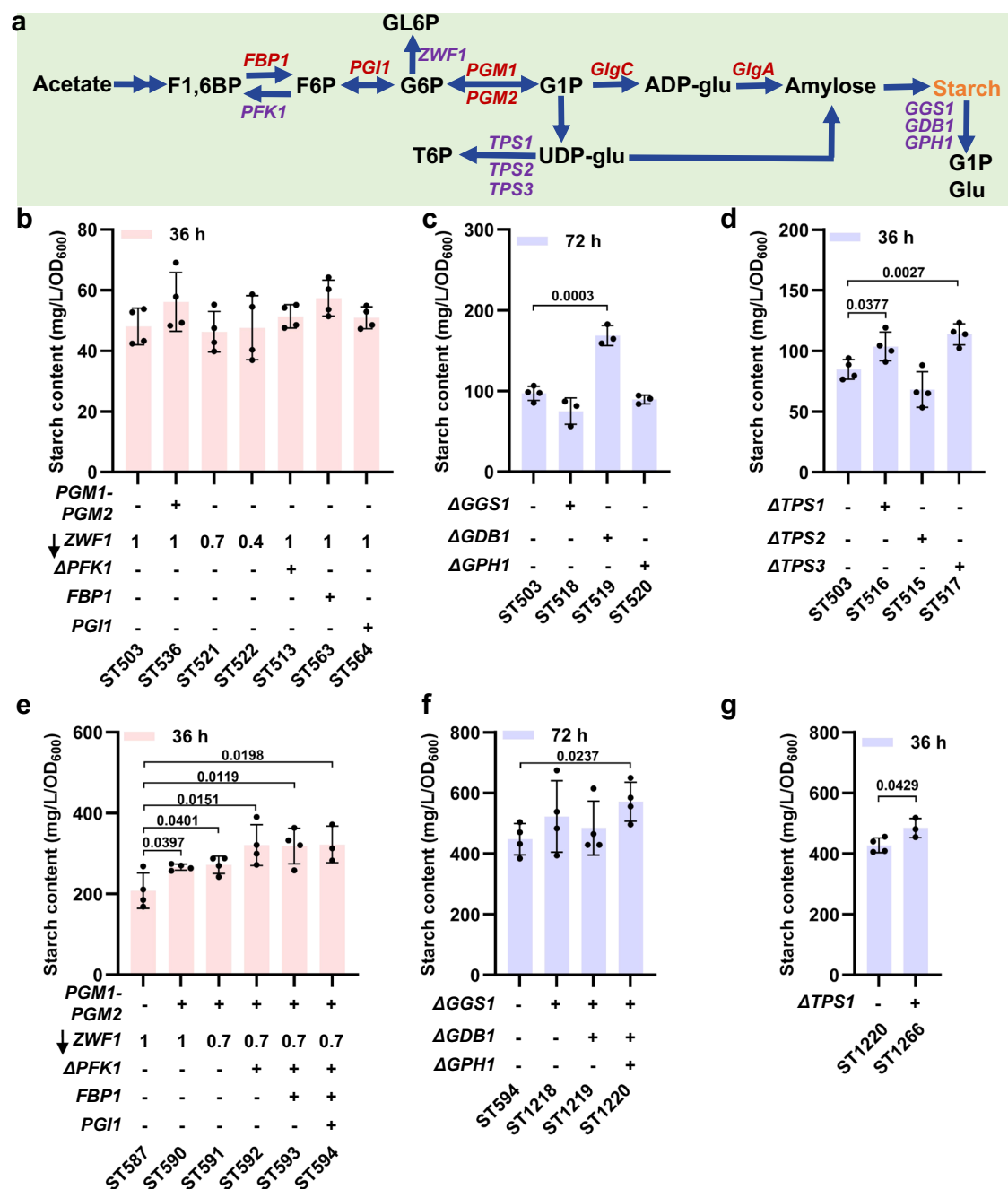
Fig. 3 | Enhanced precursor supply and reduced starch degradation improve cellular starch accumulation. a Biosynthetic pathway for starch production from acetate. Genes that were overexpressed or repressed/deleted were marked in red or purple, respectively. **b–g** Starch content in low starch producing strain (ST503, **b–d**) and high starch-producing strains ST587 (**e**), ST594 (**f**), and ST1220 (**g**), engineered for enhanced glucose-1-phosphate supply, reduced starch degradation, and decreased UDP-glucose diversion. F1,6BP D-fructose 6-phosphate, F6P fructose 6-phosphate, G6P glucose 6-phosphate, GL6P gluconolactone 6-phosphate, G1P glucose 1-phosphate, Glu glucose, T6P trehalose 6-phosphate, PGI1 Glucose-6-phosphate isomerase, PGM1 Phosphoglucomutase (alpha-D-glucose-1,6-bisphosphate-dependent), PGM2 Phosphoglucomutase. Data shown are mean values ± SDs of biological replicates (**b** ($n = 4$), **c** ($n = 3$ or 4), **d** ($n = 4$), **e** ($n = 3$ or 4), **f** ($n = 4$), **g** ($n = 3$ or 4)). **b–g** Statistical difference was determined by a two-tailed unpaired t-test. Source data are provided as a Source Data file.

Figs. 13 and 14) in ST587 and ST1271 cells, respectively. More surprisingly, the starch composition was divergent - the resistant starch fraction in the engineered strains varied from 0.99% to 23.00% (Fig. 5b). The fraction of non-resistant starch, especially the lowly polymerized dextrin, was decreased along with the increase in resistant starch fraction across the uncontrolled small-scale cultivation of all cell culture (Fig. 5b). These results suggested a time-course conformational change of starch products relevant to the metabolic/physiological reconfiguration in the engineered strains.

We further grew the ST1271 strain to explore its capacity to form starch-rich micro-grain in a bioreactor by supplying acetate and simple mineral salts. The strain accumulated 19.30 g/L starch (29.60% of the dry cell weight) after cultivation of 120 h (Fig. 5c). The resulting spatial-temporal starch productivity was 243.70 g/m²/d, representing ~50-fold higher rate than that of wheat/maize/rice cultivation (Table 1). The starch titer (19.30 g/L) and rate (160.83 mg/L/h) through the micro-grain cultivation were also an order of magnitude higher than the starch production in other microbes such as
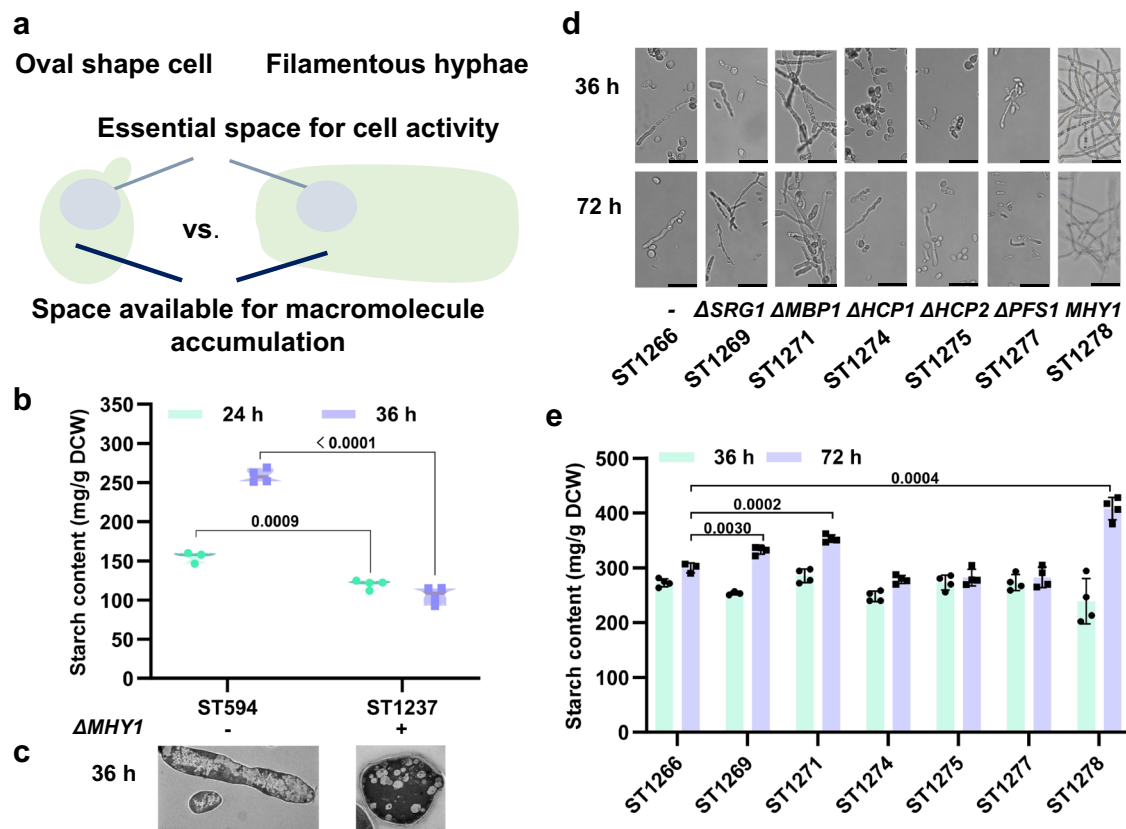
Fig. 4 | Hyphae morphology enables a larger cellular space for improved starch accumulation. a Comparison of cellular space between cells with different morphologies and sizes. **b** and **c**, Starch production and scanning electron microscopy images (scale bar = 20 μm) of strains with the dimorphic cell shape (ST594) or solely oval shape cell (ST1237). **d** and **e** Microscopic images (scale bar = 25 μm) and starch production of strains engineered for altered cell morphology. *SRG1* stress-responsive gene, *MBP1* DNA binding component of the SBF complex (Swi4p-Swi6p), *HCP1* subunit of the heterohexameric cochaperone prefoldin complex, *HCP2* subunit of the heterohexameric cochaperone prefoldin complex, *PFS1* prefoldin subunit 3, *MHY1* stress-responsive transcriptional activator. Data shown are median values with interquartile range (IQR) and distribution of biological replicates (**b**, *n* = 3 or 4), representative images (**c**, **d**), or mean values ± SDs of biological replicates (**e**, *n* = 3 or 4). Statistical difference was determined by a two-tailed unpaired *t*-test. Source data are provided as a Source Data file.

microalgae and engineered yeasts (Table 2). The micro-grain produced through fed-batch fermentation contained a steady fraction of lowly and highly polymerized starch but no resistant starch (Fig. 5d). The different starch composition patterns in micro-grain produced through distinct cultivation processes was reproducible (Supplementary Fig. 15), indicating the potential of producing micro-grain with customized starch composition through engineering of strain and fermentation process.

To extend the application of the synthetic *Y. lipolytica* strain ST1271 beyond acetate-based starch synthesis, we established a microbial straw-to-starch conversion route (Fig. 5e) by supplying acetate in combination with hydrolyzed straw-derived glucose. The strain could not grow in the medium containing glucose as the sole carbon source (Supplementary Fig. 16); however, it was able to convert glucose into starch-rich micro-grains in the presence of acetate (Supplementary Figs. 17, 18, and 19), enabling an up to 2.8-fold enhancement in carbon-to-starch yield compared to acetate alone (Supplementary Fig. 18b). This result suggests a synergistic effect between acetate and glucose in promoting both cell growth and starch synthesis, potentially through the interplay of metabolic pathways regulating energy balance or precursor availability. Cultivation in alkaline-pretreated and enzymatically hydrolyzed corn stover with acetate resulted in a starch titer of 3.40 g/L and a carbon substrate-to-starch yield of 184.02 mg/g in small-scale systems (Fig. 5f and Supplementary Fig. 20), showcasing the feasibility of this innovative straw-to-starch bioconversion.

Remodeled cellular machinery ensuring high-level starch biosynthesis

The engineered yeast cells converted two-carbon substrate acetate to macromolecule starch at superior-to-nature levels. The reprogrammed acetate-to-starch transformation process was executed in a narrow microbial cell space and associated with the global metabolism, which is largely unlike that in crops specifically focusing on the conversion of leaf-derived hexose to starch in the kernel. We are very curious about the underlying mechanism and key regulators to coordinate the engineered yeasts' response and ensure the high starch accumulation, and therefore, we performed the metabolomic and transcriptomic analysis (Supplementary Fig. 21).

We surprisingly observed that the intermediate metabolites toward starch, involved in the acetate assimilation, glyoxylate cycle, and gluconeogenesis pathways, were all dramatically decreased in ST587 and ST1271 strains (Fig. 6a and Supplementary Data 1) with the reduction margin proportional to the increased starch level. The significant reduction in central metabolites was accompanied by the differential metabolites (Supplementary Table 2 and Supplementary Fig. 22) in key metabolic pathways originating from the central metabolites (Supplementary Figs. 23 and 24): including hexose (Supplementary Fig. 24a), nucleotide (Supplementary Fig. 24b), glycerophospholipid (Supplementary Fig. 24c), fatty acid (Supplementary Fig. 24d), and amino acid metabolism (Supplementary Fig. 24e), showing a decrease in main fatty acids stearic acid and oleic acid (Supplementary Fig. 24d) occupying 80% of the total lipid[24] and in 15
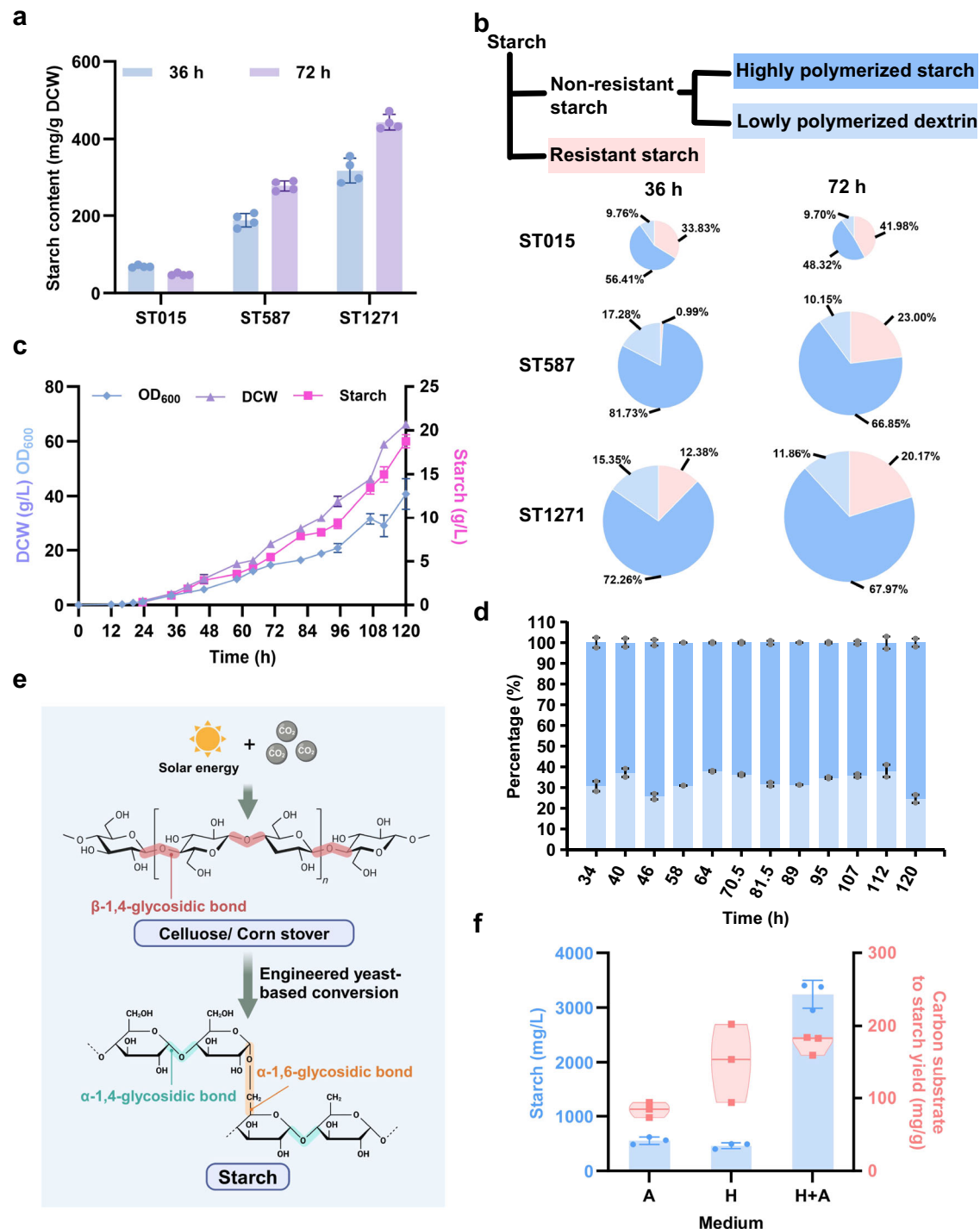
Fig. 5 | Starch production and composition profiles in micro-grain produced through low-carbon microbial manufacturing. a and **b** Total starch production and starch composition in engineered cell cultured in MMA through shake flask cultivation. **c** and **d** Starch production and starch composition of ST1271 strain cultivated in MMA via fed-batch fermentation. **e** Schematic illustration of starch production from low-carbon corn stover feedstock through an engineered yeast-based conversion. [Created in BioRender. Shi, Z. (2025) https://BioRender.com/g62b742]. **f** Starch production and carbon source-to-starch yield of ST1271 strain cultivated in A, H, and H + A media for 132 h. ST1271 was cultivated in MM containing various 6.7 g/L acetate (A), corn stover hydrolysate (H, containing 12.60 g/L glucose and 0.25 g/L acetate), or corn stover hydrolysate and 6.7 g/L acetate (H + A). Data shown are mean values ± SDs of biological replicates (**a** (n = 4), **c** and **d** (n = 2), **f** (n = 3)), or mean values of biological replicates (**b**, n = 3 or 4). Carbon to starch yield data are presented as median values with interquartile range (IQR) and distribution of biological replicates (**f**, n = 3). Source data are provided as a Source Data file.

amino acids out of total 20 (Supplementary Fig. 24e). These results indicated that the high-level starch-producing yeast cell depleted the intermediate metabolites in the main biosynthetic pathway toward starch and forged a responsive metabolomic profile for high-level starch synthesis.

The transcriptional analysis (Supplementary Figs. 25 and 26) showed a simultaneously lower expression of genes involved in acetate transport, acetate assimilation, and gluconeogenesis in ST587 and ST1271, two high-level starch-producing strains (Fig. 6a, Supplementary Figs. 27 and 28, and Supplementary Data 2), partially explaining

Table 1 | Comparison of production metrics of various starch production routes

Feedstock	Terrestrial crop, aquatic plant, or strain	Starch content (%) in grain or micro-grain	Spatial-temporal productivity (g/m²/d)	Reference *
CO₂ + light	Spring wheat	60–70	5.0	48
	Winter wheat		2.3	
CO₂ + light	Maize	65–75	5.9	49
CO₂ + light	Wild rice	68.7–87	5.6	50
	White rice		6.4	
CO₂ + light	Duckweed	75.9	9.4	51
Acetate (CO₂ + electricity)	*Yarrowia lipolytica*	29.6	243.7	This work

* The calculation of spatial-temporal starch productivities of terrestrial crops and yeast was detailed in the Methods section.

Table 2 | Comparison of microorganisms-based starch production metrics

| Feedstock	Strain	Starch content (%)	Titer (g/L)	Rate (mg/L/h)	Reference
CO₂ + light	*Synechococcus elongatus* PCC 7942	34	NA	NA	52
CO₂ + light	*Chlorella vulgaris Beijerinck*, strain CCALA 924	4–60	~5.5	35	53
CO₂ + light	*Chlorella* sp. AE10	60.3	1.87	12.96	54
Glucose + light	*Platymonas helgolandica*	39.79	3.88	16.7	55
Glucose	*Chlorella* sp. MBFJNU-17	37.97-57.60	NA	NA	56
Acetate+light	*Chlamydomonas reinhardtii*	4.3–17.3	0.031-0.238	0.062-0.431	57
Galactose + yeast extract and peptone	*Saccharomyces cerevisiae*	~8	NA	NA	58
Galactose + yeast extract and peptone	*Saccharomyces cerevisiae*	~12.5	NA	NA	59
Galactose/glucose/ethanol + yeast extract and peptone	*Saccharomyces cerevisiae*	NA	0.92	7.7	13
	Saccharomyces cerevisiae	5.7	0.34	2.9	13
Methanol + yeast extract and peptone	*Pichia pastoris*	NA	0.12	9.8	13
Acetate	*Yarrowia lipolytica*	47.18*	1.38	19.17	This work
Acetate	*Yarrowia lipolytica*	29.60 #	19.30	160.83	This work

* Tube fermentation
# 1.3 L fermenter

why only simultaneous overexpression of gluconeogenesis genes instead of single manipulation improved starch production. Moreover, the upregulation of genes for G3P-to-G6P conversion (downstream of gluconeogenesis pathway) in ST1271 strain was accompanied by increased expression of genes in the glyoxylate cycle, which supply metabolites for subsequent gluconeogenesis initiation (Fig. 6a). These data suggested that a low carbon assimilation and conversion rate might be beneficial to ensure high-level starch synthesis and there might exist automatic gene expression coordination for central metabolite conversion.

We also observed the upregulation of hyphal development-related TFs (Fig. 6b) in the high-level starch-producing strains, highlighting that the engineering strategy on morphology was reasonable and indicating that the other transcriptional changes may point out a new engineering direction for further strain design. Functional genes (Supplementary Figs. 25e and 6c) and transcriptional activators (Fig. 6b) for amino acid biosynthesis were largely downregulated. As well, TFs for activating the utilization of amino acid as a nitrogen source and ribosome biogenesis (Fig. 6b) and ribosomal components for protein translation (Supplementary Figs. 29 and 6c) were dramatically repressed. In the meantime, peptidase genes for peptide degradation and amino acid recycling were upregulated (Fig. 6c). These results altogether suggested that the engineered strains may responsively form an amino acid-centered nitrogen metabolism (amino acid synthesis, consumption, and recycling) to squeeze the resource allocation to protein and thereby supply more building blocks for starch synthesis. We further validated this by verifying a lower protein content in the engineered strains (Fig. 6d, e).

The biological cell consists of three main macromolecules: polysaccharides, proteins, and lipids, which are synthesized via natural metabolism. The change in the nitrogen-amino acid-protein synthesis bioprocess chain suggested that reallocating cellular resources may act as a possible auto-regulatory and artificial engineering strategy to strengthen starch synthesis. This hypothesis was additionally supported by decreased lipid content (Fig. 6f) and the responsive downregulation of genes for lipid/fatty acid biosynthesis (Supplementary Fig. 24d) in high-level starch strains, including *ACC1* and *FAS*. We attempted to validate this hypothesis by modulating lipid metabolism since the key regulators are several concrete ones, while those for protein synthesis are numerous and largely unclear. We first downregulated *ACC1* expression via promoter swapping in low starch-producing strain and confirmed *ACC1* expression at a specific low level (dosage-dependent) as beneficial for improved starch production (Fig. 6g, h and Supplementary Fig. 30). The *ACC1* and *FAS* downregulation manipulations based on promoter swapping were unsuccessful in high starch-producing strains after multiple attempts, indicating that a sensitive modulation of cell growth and starch synthesis was essential. We further applied CRISPR interference of *ACC1* and an inhibitor chemical of fatty acid synthase (FAS), cerulenin[25], in high starch-producing strains to reduce lipid accumulation. *ACC1* CRISPRi did not change starch production (Supplementary Fig. 31), while cerulenin treatment increased starch accumulation in a strain background-dependent manner (Supplementary Fig. 32, Fig. 6i, and Supplementary Fig. 33), altogether indicating the importance of resource reallocation and the need to fine-tune macromolecule metabolism to ensure the improvement of starch production.
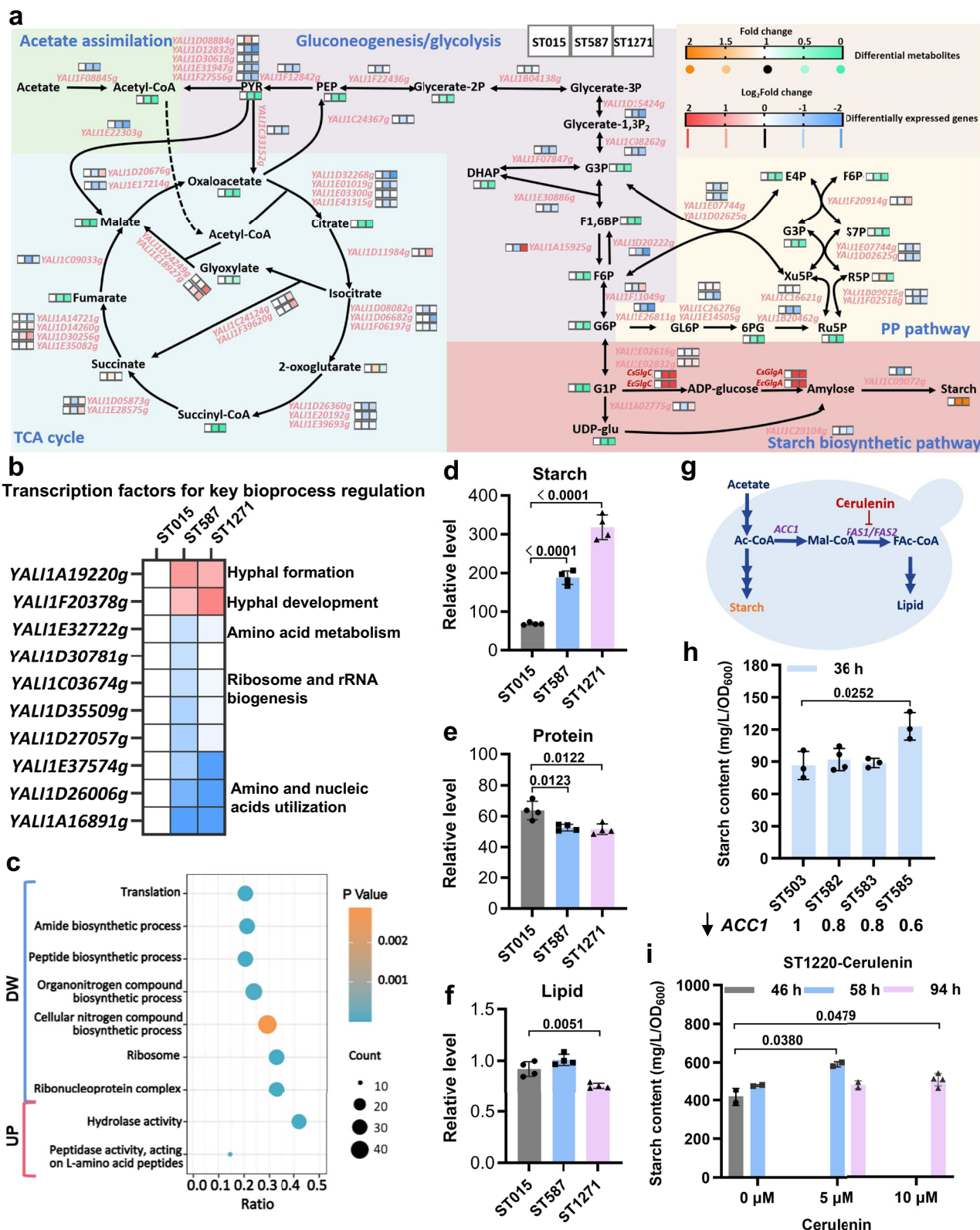
Discussion

Here, we engineered cell metabolism and morphology to transform oleaginous yeast *Y. lipolytica* cell to starch-rich micro-grain and established an arable land-independent route for the high-level production of customized starch through low-carbon microbial manufacturing.

The established process combined engineered yeasts and electricity to convert CO_2 to starch, highlighting the superior efficiency of the hybrid electrochemical-bioconversion approach[26]. The process directly generated starch-rich micro-grain in comparison to the kernel, which is a part of the crop biomass, presenting an ~50 time (243.7 vs. <6.4 g/m^2/d) higher spatial-temporal productivity and 8.1 time higher

Fig. 6 | Metabolomic and transcriptomic analysis to elucidate the cellular response ensuring high-level starch production. a Comparison of metabolites and gene expression for central biosynthetic pathways for acetate-to-starch conversion in engineered strains ST587 and ST1271. **b** Transcription factors with the greatest expression changes. **c** GO enrichment of differentially expressed genes relating to amino acid metabolism and protein synthesis. **d–f** Cellular macromolecule comparison of the engineered strains. **g** Brief illustration of key nodes in the lipid biosynthetic pathway. **h** Starch content of strains engineered for decreased *ACC1* expression. **i** Starch content of ST1220 strain treated with cerulenin. Starch content comparisons were conducted at different time points due to the growth inhibition caused by the addition of cerulenin (Supplementary Fig. 32).

Data shown are a comparison of omics data of quadruplicates (**a–c**) or mean values ± SDs of biological replicates (**d–f** ($n = 4$), **h** ($n = 3$ or 4), **i** ($n = 2$ or 4)). Statistical difference was determined by a two-tailed unpaired *t*-test. PYR pyruvate, OAA oxaloacetate, 2-OG 2-oxoglutarate, PEP phosphoenolpyruvate, Glycerate-2P glycerate 2-phosphate, Glycerate-3P glycerate 3-phosphate, Glycerate-1,3P2 glycerate 1,3-diphosphate, G3P glyceraldehyde 3-phosphate, DHAP dihydroxyacetone phosphate, 6PG gluconate 6-phosphate, Ru5P ribulose 5-phosphate, Xu5P xylulose 5-phosphate, R5P ribose 5-phosphate, S7P sedoheptulose 7-phosphate, E4P erythrose 4-phosphate, G1P glucose 1-phosphate, ADP-glu ADP-glucose, UDP-glu UDP-glucose. Source data are provided as a Source Data file.

energy efficiency than the crop planting: >2.82% vs. solar-to-corn kernel efficiency 0.31%[14].

The high starch content in micro-grain cultivated with short-chain carbon (C1-C4) feedstock, 47.18%, was achieved through a synthetic biology-driven strain customization, which mimicked the crop domestication at a much faster rate (months vs. thousand years). As a supplementary alternative to the traditional reverse genetics approach to understanding natural starch biosynthesis machinery in plants, our work demonstrates a build-to-learn means to dissect the key regulators and molecular mechanisms determining macromolecule synthesis and cell fate. In creating artificial cells accumulating high-level starch via the C2-C3-C6-C6n bioconversion pathway, we highlighted the essentiality of high-level expression of SBP genes and combinatorial manipulation of conserved gluconeogenesis pathway in ensuring efficient starch biosynthesis. In addition, our work dissect that global metabolism remodeling, cellular resource reallocation (together with previous studies[27–29]), and cell size regulation were generally applicable strategies to determine macromolecule accumulation and composition. More importantly, in contrast to the fact that the abovementioned processes were complicatedly interconnected with seedling growth and controlled by various genes in crops[30–32], those processes can be modulated by manipulation of limited genes, enabling the easiness to allow for a much faster innovation speed for iterative micro-grain improvement.

Via the systematic engineering of yeast cells and cultivation condition control, we obtained a variety of micro-grains with different macromolecules (starch-protein-lipid ratio) and starch compositions, which could be readily incorporated into downstream application (Supplementary Discussion 1). We prospect that, with the increasingly gained knowledge and development of synthetic biology tools, it will soon be possible to modulate specific features of the micro-grain ingredient (such as starch hardness, stickiness, and gelatinization) and even develop micro-grain to desired full-nutrient food resource, for instance, customized nutritional powder. Additionally, further technological advancements and resource integration are needed to address the high cost of the CO_2-acetate-starch route at this stage (Supplementary Discussion 2 and 3, Supplementary Method 1) and improve the process efficiency and scalability.

Methods
Strain construction
Escherichia coli DH5α was employed as a host for plasmid construction and propagation. *Yarrowia lipolytica* strains (Supplementary Data 3) for this study were all derived from W29 (NRRL Y-63746). The genetically engineered strains were constructed with ST015, a W29-derived strain carrying *Cas9* and *HygR* (hygromycin marker) genes in the *KU70* locus[33]. The strain manipulation was performed with either a Cas9-assisted approach[34] or dCpf1/dCas12-mediated gene depression[35]. Specifically, for gene deletions, plasmids containing gRNAs targeting the gene of interest (including a marker gene: *NatMX*) and donor fragments were required. The donor fragments were generated through overlap PCR to fuse the upstream (~500 bp) and downstream (~500 bp) regions of the target gene. For gene

integration, plasmids containing gRNAs targeting specific integration sites (also including a marker gene: *NatMX*) and the integration fragments were used. The integration fragments were first obtained by PCR amplification of the target gene. This fragment was then cloned into a plasmid containing homologous arms for the integration site. The plasmid was digested to isolate the integration fragment for further use. For gene repression, a strategy was employed that involved replacing weak promoters using a Cas9-based system or, alternatively, designing gRNAs targeting the gene of interest for repression based on dCpf1. Yeast transformation was carried out using the lithium acetate method, and transformants were validated through colony PCR.

Plasmids (Supplementary Data 4) were constructed using Gibson assembly with GenBuilder™ cloning kit (Genscript). The genes manipulated in this work were obtained via PCR (Supplementary Data 5) with either synthesized gene (Genscript) or W29 genome as the template for heterologous genes (Supplementary Data 6) and native genes (Supplementary Table 3), respectively. DNA fragments for gene deletion and genome integration were constructed by overlap PCR[36] or by enzyme digestion of pre-assembled plasmids.

Media and strain cultivation
E. coli strains were grown at 37 °C on Luria-Bertani (LB) medium/plate containing 100 mg/L ampicillin. *Y. lipolytica* strains were maintained on YPD (10 g/L yeast extract, 20 g/L peptone, 20 g/L glucose) medium or YPD solid plates supplemented with 20 g/L agar. Recombinant *Y. lipolytica* transformants were selected using YPD plates supplemented with 250 mg/L nourseothricin.

For routine strain evaluation, strains were cultivated in mineral/DELFT medium (MM)[37] containing 27.3 g/L sodium acetate (corresponding to 20 g/L acetic acid) as the sole carbon source (MMA), pH 6.0. For the evaluation of promoter strength, both MMA and MM containing 20 g/L glucose as the sole carbon source (MMG) were used. To assess ATP enhancement effects, MMA was supplemented with 5 g/L sodium tripolyphosphate $Na_5P_3O_{10}$, 5 g/L sodium hexametaphosphate $(NaPO_3)_6$, or formate (0.1, 0.5, or 1 g/L). To inhibit fatty acid synthase (FAS) activity, MMA was supplemented with 5 or 10 μM cerulenin. To evaluate the effect of acetate/acetic acid source on cell growth and starch production, commercial and electrosynthetic acetic acid were used as the carbon source in MMA for the data collection of Fig. 2f. Whereas, for the rest strain cultivation using MMA, commercial sodium acetate or acetic acid (carbon feed for the fed-batch fermentation) were used as the carbon source.

Strains were cultivated at 30 °C in 48-deep well plates at 700 rpm in a high-speed shaker (ZQZY-BB8E, Shanghai Zhichu, China) (Supplementary Fig. 1), 12 mL cultivation tubes at 220 rpm, or 250 mL shake flasks at 220 rpm in a shaking incubator (ZQZY-AF8 Shanghai Zhichu, China) (Figs. 2b, c, 4b, e, 5a, Supplementary Figs. 9, 12a, b, 13, 14, and 15a).

The standard cultivation process began by pre-culturing cells from agar plates into either 800 μL of medium in 48-deep well plates or 2.5 mL of medium in 12 mL tubes. Pre-cultures were then inoculated into fresh media at an initial OD_{600} of 0.05. OD_{600} and starch measurements were taken after 24, 36, or 72 h, depending on the impacts

that were meant to quantify. If pre-cultivation and sub-cultivation media had different carbon sources, pre-cultured cells were washed with sterile water before inoculation.

Fed-batch fermentation

Fed-batch fermentation began with inoculation of single colonies into 2.5 mL of MMA for 60 h of pre-cultivation. These pre-cultures were transferred into 50 mL of fresh medium, and the resulting cultures were used to inoculate bioreactors to an initial OD_{600} of 0.1.

Fed-batch fermentations were conducted in a 1.3 L Eppendorf DASGIP Parallel Bioreactors System equipped with pH, dissolved oxygen (DO), and temperature probes. DO was maintained at 20% using a two-level cascade of stirring (400–1600 rpm) and airflow (24–220 sL/h). The fermentation was conducted at 30 °C, with pH controlled between 5.75 and 6.25 via automatic addition of 6 M KOH or 3 M HCl. The reactors initially contained 0.4 L of MMA. One liter of medium contained 7.5 g $(NH_4)_2SO_4$, 14.4 g KH_2PO_4, 0.5 g $MgSO_4·7H_2O$, 27.3 g sodium acetate, 2 mL trace metals solution, 1 mL vitamin solution, and 1.5 mL antifoam. Stirring and aeration rates were initially set at 400 rpm and 24 sL/h, respectively. Feeding began when acetic acid levels fell below 5 g/L. The feed medium was divided into two pumps: one delivering pure acetic acid and the other a solution containing 65.625 g/L $(NH_4)_2SO_4$, 26.25 g/L KH_2PO_4, 4.375 g/L $MgSO_4·7H_2O$, 70 mL/L trace metals solution, and 35 mL/L vitamin solution. Sampling was performed four times daily to measure OD_{600}, DCW, acetic acid, and starch. All sampling and tests were performed in biological duplicate.

Calculation of the ATP consumption for acetate-to-starch conversion

The CAVE online platform was utilized to calculate ATP consumption for acetate-to-starch conversion[38]. Initially, the *Y. lipolytica* genome-scale metabolic (GEM) model, iYli212[39], was uploaded to the platform. Subsequently, the ATP and ubiquinol-6 supply reactions were incorporated into the model as follows: ATP_$C_{10}H_{16}N_5O_{13}P_3$ < = > ADP_$C_{10}H_{15}N_5O_{10}P_2$ + phosphate_H_3O_4P, and 2.0 H + _p + 1 + ubiquinone-6_$C_{39}H_{58}O_4$ < = > ubiquinol-6_$C_{39}H_{60}O_4$. Acetate was then set as the substrate, and ADP-glucose as the target product for the calculation of ATP demand through the flux balance analysis (FBA)[40].

Starch production from corn stover hydrolysates

Corn stover hydrolysate supplied by Prof. Guodong Liu was generated by alkaline pretreatment and enzymatic hydrolysation. The hydrolysate contains 68 g/L glucose, 3 g/L acetate, and 32 g/L xylose. The hydrolysate was diluted fourfold with deionized water to prepare the working medium. The diluted hydrolysate was then mixed with MM containing 7.5 g/L $(NH_4)_2SO_4$, 14.4 g/L KH_2PO_4, 0.5 g/L $MgSO_4·7H_2O$, 2 mL/L vitamin solution, and 1 mL/L trace metal solution, pH 6.0 (referred to as H medium). 6.7 g/L acetate was added to the H medium to make the H + A medium.

Scanning electron microscopy

The ST594 and ST1237 strains were cultured in MMA medium for 36 h. Cells were harvested and washed twice with phosphate-buffered saline (PBS) to remove any residual media. Fixation was performed overnight at 4 °C using 2.5% glutaraldehyde. After fixation, cells were washed three times with buffer, each wash lasting 10 minutes, to ensure the removal of residual glutaraldehyde. After centrifugation, cells were immersed in 1% osmium tetroxide for 1 h for secondary fixation, followed by three buffer washes. For dehydration, cells were treated with an ethanol gradient (30%, 50%, 75%, 95%, and 100%), each step lasting 15 min. Ethanol was gradually replaced by an embedding agent through incubation in solutions of increasing concentrations. The embedded samples were sectioned and mounted onto copper grids,

then stained with 2% uranyl acetate for 15 min, followed by 1% lead citrate for 30 s. High-resolution imaging of cell surface structures was conducted using a Hitachi HT7700 transmission electron microscope at the appropriate accelerating voltage.

Cell growth assessment

Growth was assessed by measuring OD_{600} using a microplate reader (BioTek Synergy LX, Agilent, USA) or by determining the dry cell weight (DCW) by weighing >5 mL of cells dried to a constant weight at 85 °C.

Fluorescence measurement

The hrGFP fluorescence (λ excitation 488 nm, λ emission 530 nm, Gain 100) was measured using a microplate reader (BioTek Synergy MX, Agilent, USA). Relative fluorescence intensity was calculated by dividing the fluorescence value by OD_{600}[41].

Starch quantification

Micro-grain processing and starch quantification were performed using Rapid Total Starch (RTS) (Figs. 2–4, 5b, d, 6d, h, i, Supplementary Figs. 2–12, 13d–f, 14–15, 30, 31, 33, and 34) and RTS-NaOH (Figs. 5a–d, f, Supplementary Fig. 13a–c, 15, 18b, and 34) methods, respectively. A total of 2 mL of fresh yeast culture was collected and washed twice with distilled water to give the yeast pellet for subsequent treatment.

For the process using the RTS method, the yeast pellet was resuspended in 1.5 mL of distilled water and vortexed for 10 minutes with 0.4–0.6 mm glass beads to disrupt the cells. For the quantification of non-resistant starch, the cell lysate was mixed with reagents (including α-amylase and amyloglucosidase enzymes and sodium acetate buffer (100 mM, pH 5.0) plus calcium chloride (5 mM)), and enzymatically degraded into glucose using the Total Starch Assay Kit (NEOGEN Megazyme, K-TSTA-100A) following the manufacturer's instructions. For the quantification of low-polymerized dextrins (a fraction of non-resistant starch), the cell lysate was treated using the same procedure as for non-resistant starch but with amyloglucosidase as the sole enzyme during the starch degradation process. The released glucose content was quantified using the Liquid Sample Glucose Content Assay Kit (GOD-POD).

For the quantification of total starch (comprising both resistant and non-resistant starch) using the RTS-NaOH method, the yeast pellet was mixed with 0.05 mL of 80% (v/v) ethanol and vortexed to ensure complete wetting and dispersion of the sample. Then, 0.5 mL of 1.7 M sodium hydroxide solution was added, and the mixture was vortexed for 15 min. The resulting cell lysate was mixed with reagents (including α-amylase and amyloglucosidase enzymes and sodium acetate buffer (600 mM, pH 3.8) plus calcium chloride (5 mM)) and enzymatically degraded into glucose using the same kit following the manufacturer's instructions. The glucose content was quantified using the Liquid Sample Glucose Content Assay Kit (GOD-POD).

The accuracy of these methods was validated by quantifying a starch standard with a defined composition (resistant starch: 47.4%, non-resistant starch: 35.9%, Megazyme, resistant starch control in K-RAPRS kit) (Supplementary Fig. 34).

Acetate and glucose determination

The cell culture was mixed with an equal volume of 14 mM H_2SO_4, vortexed, and centrifuged at 9600 g for 2 min. The supernatant was analyzed using an HPLC system equipped with an HPX-87H column (Bio-Rad Laboratories, Inc.), using 14 mM H_2SO_4 as the mobile phase at 0.6 mL/min flow rate for 20 min. The column oven was maintained at 60 °C, and a 20 μL sample was injected. The Refractive Index Detector (RID-20A) was used for metabolite detection. The metabolite concentrations were quantified by comparison with reference standards.

Protein and lipid quantification

Protein content was determined using a modified biuret method[42]. The relative lipid comparison between the strains was performed by processing the fatty acid data in the metabolomics dataset using the procedure described as follows. The numbers of the proportions of main fatty acids were collected from previous report[24]: C16:1 (6%), C16:0 (11%), C18:1 (61), and C18:0 (14%). The fold change values of C16:1, C16:0, C18:1, and C18:0 fatty acids in ST587 and ST1271 were calculated relative to the average values in ST015. Each fold change value was then multiplied by the corresponding proportion of its fatty acid, yielding a weighted value for each fatty acid. The sum of these weighted values represented the relative expression of lipids.

RNAseq-guided identification of strong promoters under the acetate condition

RNAseq samples were prepared by cultivating strain ST015 in MMA in tubes for 16 h (log phase). Cell pellets were collected by centrifugation at 240 g and washed twice with PBS. RNA extraction, library construction, and sequencing processes were performed by Majorbio Biotech. Clean reads were aligned to the reference genome (GCA_001761485.1) using HISAT2 software. FeatureCounts tool was used to count reads per gene, and read numbers per kilobase of gene length were calculated. The promoters of the eight genes with the highest read counts per kilobase were selected for subsequent evaluation of promoter strength. The promoters of two types of length, 500 bp and 1200 bp, were fused with hrGFP, Lip2 terminator, and homology arms to generate DNA fragments for integrative expression of hrGFP in genomic C2 site[43]. The resulting strains were cultivated in MMG and MMA for 24 or 25.5 h for quantification of fluorescence, which quantitatively indicates the driving force of selected promoters.

Transcriptomic and metabolomic analysis

Transcriptomic and metabolomic samples were prepared by cultivating strains in MMA medium in shake flasks for 36 h. Biological quadruplicates were performed for each strain (ST015, ST587, and ST1271). Cell pellets were collected from 2 mL of culture by centrifuging at 240 g and washed twice with PBS.

For transcriptomic analysis, RNA extraction, library construction, and sequencing were conducted by BiotreeDB Biotech. Clean reads were aligned to the reference genome (GCA_001761485.1) using HISAT2 software, and gene expression levels were quantified using the featureCounts tool, resulting in FPKM values for each sample. Principal component analysis (PCA) of gene expression (FPKM) was performed to assess inter-group differences and reproducibility. Differentially expressed genes between groups (ST587 vs. ST015, ST1271 vs. ST015, and ST1271 vs. ST587) were identified using DESeq2 with thresholds of |log2(FoldChange)| ≥1 and padj ≤0.05. Visualization of differentially expressed genes was achieved using volcano plots, and hierarchical clustering of FPKM values was performed with R software. Functional enrichment analysis, including Gene Ontology (GO) and KEGG pathway enrichment, was conducted using the clusterProfiler package.

For the metabolomic analysis, metabolite extraction, identification, and data processing processes were performed by BiotreeDB Biotech. The process includes metabolite extraction, metabolite analysis and data processing[44,45]. Metabolite Extraction: Samples were mixed with water, homogenized, and ultrasonicated in an ice-water bath. After protein quantification, they were extracted using a 1:1 methanol-water solution, followed by vortexing, ultrasonication, and centrifugation. The supernatants were pooled, dried, reconstituted, and prepared for subsequent analysis. Metabolite Analysis: Metabolites were separated using a Vanquish ultra-high-performance liquid chromatograph equipped with a Waters ACQUITY UPLC BEH Amide column. Mobile phase A consisted of an aqueous solution with 25 mmol/L ammonium acetate and 25 mmol/L ammonia water, while mobile phase B was acetonitrile. The sample plate temperature was

maintained at 4 °C, with an injection volume of 2 μL. Data Processing: Mass spectrometry data were converted using ProteoWizard and processed using XCMS in R for peak detection and alignment[46]. metabolites were annotated using BiotreeDB with a threshold cutoff of 0.3 (Supplementary Data 7). Data Analysis: The raw data, including three quality control (QC) samples and twelve experimental samples, were pre-processed to filter outliers. Principal component analysis (PCA) was performed using SIMCA software (V16.0.2), with the data log transformed and centered before modeling. Multivariate statistical analysis was conducted to identify differential metabolites, using Student's t-test with a P-value < 0.05 and OPLS-DA modeling with a Variable Importance in Projection (VIP) score >1[47]. KEGG pathway and network analyses were performed using clusterProfiler.

Calculation/estimation of spatial-temporal starch productivity and electricity-to-starch energy efficiency

Starch productivity was calculated/estimated with the following equation:

$$\text{Starch productivity}(g/m^2/d) = (\text{Grain or micro} - \text{grain titer x Starch content})/(\text{Time duration for the production x Land area employed})$$

(1)

For crop grains, the values were set to 9000 kg/hectare for production, and 110 days (spring wheat, maize, and rice) or 240 days (winter wheat) for the duration. These values represent upper and lower levels of production parameters to ensure relatively higher starch productivity for comparison with micro-grain. Starch content data for wheat (61.3%), wild rice (68.7%), and white rice (78.7%) were sourced from the USDA National Nutrient Database or selected as the typical data for maize (72%). For micro-grain, starch productivity was calculated based on starch titer (19.3 g/L), fermentation broth volume (0.6 L), fermentation duration (5 days), and land area for the 1.3 L fermenter (0.0095 m²).

Electricity-to-starch energy efficiency: The efficiency was derived by multiplying the electricity-to-acetate energy efficiency (34%[15] vs. the theoretical yield of 39.1%[14]) by the acetate-to-starch mass yield (0.054 – 0.105 g/g for ST1271 (Supplementary Table 4)). The acetate/acetic acid-to-starch yield of 0.054 g/g was calculated for fed-batch cultivation at a 1.3 L fermenter (actual value is likely higher due to acetate volatility), and the yields of 0.083 to 0.105 g/g were calculated for shake flask cultivation. We chose 0.083 g/g, the lower yield limit for shake flask cultivation, for the calculation, giving an overall energy efficiency of 2.82%.

Statistics and reproducibility

All experiments were performed in quadruplicate unless otherwise specified, and statistical differences were analyzed using a two-tailed unpaired t-test with GraphPad Prism 10.

Graphic preparation

Figure 1 was created using Microsoft PowerPoint, with elements sourced from BioRender or captured by the authors. Figures 4a and 6g were also designed in Microsoft PowerPoint. Figure 5e and Supplementary Fig. 15 were generated using BioRender.

Reporting summary

Further information on research design is available in the Nature Portfolio Reporting Summary linked to this article.

Data availability

The raw omics data generated in this study have been deposited in the NCBI Sequence Read Archive (SRA) under accession PRJNA1226773 for transcriptome raw data of ST015 strain, PRJNA1226898 for transcriptome raw data of ST015, ST587, and ST1271 strains. Metabolomics

raw data of ST015, ST587, and ST1271 strains are available at Metabo-Lights under the accession code MTBLS12252. Source data are provided with this paper.

References

1. Eliasson, A.-C. *Starch in Food: Structure, Function and Applications* 2nd edn, Vol. 916 (CRC Press, 2004).
2. INC, G.I.A. *Starch: A Global Strategic Business Report*. https://www.researchandmarkets.com/reports/2832332/starch-global-strategic-business-report?srsltid=AfmBOormil-xvuR5LPaQt0VSPK6P9xgwArIGSMMUT2ctVkVkVYk3PDTt (2024).
3. Kumar, Y. et al. Starch: current production and consumption tends. In *Starch: Advances in Modifications, Technologies and Applications*. (eds. V. S. Sharanagat, D. C. Saxena, K. Kumar & Y. Kumar) 1–10 (Springer International Publishing, 2023).
4. Kong, X. China must protect high-quality arable land. *Nature* **506**, 7–7 (2014).
5. Wang, G., Wu, X. & Yin, Y. Synthetic biology-driven customization of functional feed resources. *Trends Biotechnol.* **40**, 777–780 (2022).
6. Zhu, X.-G., Long, S. P. & Ort, D. R. What is the maximum efficiency with which photosynthesis can convert solar energy into biomass? *Curr. Opin. Biotech.* **19**, 153–159 (2008).
7. Lobell, D. B. & Gourdji, S. M. The influence of climate change on global crop productivity. *Plant Physiol.* **160**, 1686–1697 (2012).
8. Llorente, B., Williams, T. C., Goold, H. D., Pretorius, I. S. & Paulsen, I. T. Harnessing bioengineered microbes as a versatile platform for space nutrition. *Nat. Commun.* **13**, 6177 (2022).
9. Graham, A. E. & Ledesma-Amaro, R. The microbial food revolution. *Nat. Commun.* **14**, 2231 (2023).
10. Ma, S. & Kenis, P. J. Electrochemical conversion of CO_2 to useful chemicals: current status, remaining challenges, and future opportunities. *Curr. Opin. Chem. Eng.* **2**, 191–199 (2013).
11. Cai, T. et al. Cell-free chemoenzymatic starch synthesis from carbon dioxide. *Science* **373**, 1523–1527 (2021).
12. Zheng, T. et al. Upcycling CO2 into energy-rich long-chain compounds via electrochemical and metabolic engineering. *Nat. Catal.* **5**, 388–396 (2022).
13. Tang, H. et al. Metabolic engineering of yeast for the production of carbohydrate-derived foods and chemicals from C1–3 molecules. *Nat. Catal.* **7**, 21–34 (2024).
14. Hann, E. C. et al. A hybrid inorganic-biological artificial photosynthesis system for energy-efficient food production. *Nat. Food* **3**, 461–471 (2022).
15. Jin, J. et al. Constrained C(2) adsorbate orientation enables CO-to-acetate electroreduction. *Nature* **617**, 724–729 (2023).
16. EFSA Panel on Nutrition, N. F. et al. Safety of *Yarrowia lipolytica* yeast biomass as a novel food pursuant to Regulation (EU) 2015/2283. *EFSA J.* **17**, e05594 (2019).
17. Liu, N., Qiao, K. & Stephanopoulos, G. 13C Metabolic flux analysis of acetate conversion to lipids by *Yarrowia lipolytica*. *Metab. Eng.* **38**, 86–97 (2016).
18. Xue, Z. et al. Production of omega-3 eicosapentaenoic acid by metabolic engineering of Yarrowia lipolytica. *Nat. Biotechnol.* **31**, 734–740 (2013).
19. Qiao, K. J., Wasylenko, T. M., Zhou, K., Xu, P. & Stephanopoulos, G. Lipid production in *Yarrowia lipolytica* is maximized by engineering cytosolic redox metabolism. *Nat. Biotechnol.* **35**, 173–177 (2017).
20. Saez-Saez, J. et al. Engineering the oleaginous yeast *Yarrowia lipolytica* for high-level resveratrol production. *Metab. Eng.* **62**, 51–61 (2020).
21. Konzock, O. & Norbeck, J. Deletion of *MHY1* abolishes hyphae formation in *Yarrowia lipolytica* without negative effects on stress tolerance. *PloS One* **15**, e0231161 (2020).
22. Pomraning, K. R. et al. Regulation of yeast-to-hyphae transition in *Yarrowia lipolytica*. *mSphere* **3**, e00541 (2018).
23. Hurtado, C. A. R. & Rachubinski, R. A. *MHY1* encodes a C_2H_2-type zinc finger protein that promotes dimorphic transition in the yeast *Yarrowia lipolytica*. *J. Bacteriol.* **181**, 3051–3057 (1999).
24. Blazeck, J. et al. Harnessing *Yarrowia lipolytica* lipogenesis to create a platform for lipid and biofuel production. *Nat. Commun.* **5**, 3131 (2014).
25. Schmid, B., Rippmann, J. F., Tadayyon, M. & Hamilton, B. S. Inhibition of fatty acid synthase prevents preadipocyte differentiation. *Biochem. Bioph. Res. Co.* **328**, 1073–1082 (2005).
26. Crandall, B. S., Harland-Dunaway, M., Jinkerson, R. E. & Jiao, F. Electro-agriculture: Revolutionizing farming for a sustainable future. *Joule* **8**, 2974–2991 (2024).
27. Ajjawi, I. et al. Lipid production in *Nannochloropsis gaditana* is doubled by decreasing expression of a single transcriptional regulator. *Nat. Biotechnol.* **35**, 647–652 (2017).
28. Kato, Y. et al. Enhancing carbohydrate repartitioning into lipid and carotenoid by disruption of microalgae starch debranching enzyme. *Commun. Biol.* **4**, 450 (2021).
29. Li, Q. et al. Relationship, evolutionary fate and function of two maize co-orthologs of rice GW2 associated with kernel size and weight. *BMC Plant Biol.* **10**, 143 (2010).
30. Yang, W. et al. The RING E3 ligase CLG1 targets GS3 for degradation via the endosome pathway to determine grain size in rice. *Mol. Plant* **14**, 1699–1713 (2021).
31. Osnato, M. From the archives: a rice grain size regulatory module, GWAS of primary plant metabolism, and promoter trapping of polarity markers. *Plant Cell* **34**, 3485–3486 (2022).
32. Ma, B. et al. A plasma membrane transporter coordinates phosphate reallocation and grain filling in cereals. *Nat. Genet* **53**, 906–915 (2021).
33. Liu, Q. et al. Reprogramming the metabolism of oleaginous yeast for sustainably biosynthesizing the anticarcinogen precursor germacrene A. *Green. Chem.* **25**, 7988–7997 (2023).
34. Holkenbrink, C. et al. EasyCloneYALI: CRISPR/Cas9-based synthetic toolbox for engineering of the yeast yarrowia lipolytica. *Biotechnol. J.* **13**, e1700543 (2018).
35. Zhang, J. L. et al. Gene repression via multiplex gRNA strategy in *Y. lipolytica*. *Micro. Cell Fact.* **17**, 62 (2018).
36. Zhou, Y. J. et al. Modular pathway engineering of diterpenoid synthases and the mevalonic acid pathway for miltiradiene production. *J. Am. Chem. Soc.* **134**, 3234–3241 (2012).
37. Jensen, N. B. et al. EasyClone: method for iterative chromosomal integration of multiple genes in Saccharomyces cerevisiae. *FEMS Yeast Res.* **14**, 238–248 (2014).
38. Mao, Z. et al. CAVE: a cloud-based platform for analysis and visualization of metabolic pathways. *Nucleic Acids Res.* **51**, W70–W77 (2023).
39. Guo, Y. et al. Dissecting carbon metabolism of *Yarrowia lipolytica* type strain W29 using genome-scale metabolic modelling. *Comput Struct. Biotechnol. J.* **20**, 2503–2511 (2022).
40. Orth, J. D., Thiele, I. & Palsson, B. What is flux balance analysis? *Nat. Biotechnol.* **28**, 245–248 (2010).
41. Wang, G. et al. Improvement of cis,cis-muconic acid production in *Saccharomyces cerevisiae* through biosensor-aided genome engineering. *ACS Synth. Biol.* **9**, 634–646 (2020).
42. Liu, L. et al. Integrating Experimental and computational analyses of yeast protein profiles for optimizing the production of high-quality microbial proteins. *Appl. Biochem. Biotechnol.* **196**, 8741–8762 (2024).
43. Wang, G. et al. Engineering yeast *Yarrowia lipolytica* for methanol assimilation. *ACS Synth. Biol.* **10**, 3537–3550 (2021).
44. Want, E. J. et al. Global metabolic profiling procedures for urine using UPLC-MS. *Nat. Protoc.* **5**, 1005–1018 (2010).

45. Alseekh, S. et al. Mass spectrometry-based metabolomics: a guide for annotation, quantification and best reporting practices. *Nat. Methods* **18**, 747–756 (2021).

46. Smith, C. A., Want, E. J., O'Maille, G., Abagyan, R. & Siuzdak, G. XCMS: processing mass spectrometry data for metabolite profiling using nonlinear peak alignment, matching, and identification. *Anal. Chem.* **78**, 779–787 (2006).

47. Wiklund, S. et al. Visualization of GC/TOF-MS-based metabolomics data for identification of biochemically interesting compounds using OPLS class models. *Anal. Chem.* **80**, 115–122 (2008).

48. Wang, X. et al. Pre-anthesis high temperature acclimation alleviates the negative effects of post-anthesis heat stress on stem stored carbohydrates remobilization and grain starch accumulation in wheat. *J. Cereal Sci.* **55**, 331–336 (2012).

49. Liu, N., Xue, Y. D., Guo, Z. Y., Li, W. H. & Tang, J. H. Genome-wide association study identifies candidate genes for starch content regulation in zaize kernels. *Front. Plant Sci.* **7**, 1046 (2016).

50. Zhao, Y. T., Henry, R. J. & Gilbert, R. G. Starch structure-property relations in Australian wild rices compared to domesticated rices. *Carbohyd. Polym.* **271**, 118412 (2021).

51. Guo, L., Fang, Y., Jin, Y., He, K. & Zhao, H. High starch duckweed biomass production and its highly-efficient conversion to bioethanol. *Environ. Technol. Innov.* **32**, 103296 (2023).

52. Qiao, C. et al. Effects of reduced and enhanced glycogen pools on salt-induced sucrose production in a sucrose-secreting strain of *Synechococcus elongatus* PCC 7942. *Appl. Environ. Microbiol.* **84**, e02023–17 (2018).

53. Branyikova, I. et al. Microalgae-novel highly efficient starch producers. *Biotechnol. Bioeng.* **108**, 766–776 (2011).

54. Cheng, D. et al. Improving carbohydrate and starch accumulation in *Chlorella sp.* AE10 by a novel two-stage process with cell dilution. *Biotechnol. Biofuels* **10**, 75 (2017).

55. Shi, Q., Chen, C., He, T. & Fan, J. Circadian rhythm promotes the biomass and amylose hyperaccumulation by mixotrophic cultivation of marine microalga *Platymonas helgolandica*. *Biotechnol. Biofuels Bioprod.* **15**, 75 (2022).

56. Xiao, X. et al. A novel two-stage heterotrophic cultivation for starch-to-protein switch to efficiently enhance protein content of *Chlorella sp.* MBFJNU-17. *Bioresour. Technol.* **344**, 126187 (2022).

57. Figueroa-Torres, G. M., Pittman, J. K. & Theodoropoulos, C. A highly productive mixotrophic fed-batch strategy for enhanced micro-algal cultivation. *Sustain. Energy Fuels* **6**, 2771–2782 (2022).

58. Pfister, B. et al. Tuning heterologous glucan biosynthesis in yeast to understand and exploit plant starch diversity. *BMC Biol.* **20**, 207 (2022).

59. Pfister, B. et al. Recreating the synthesis of starch granules in yeast. *Elife* **5**, e1555 (2016).

Acknowledgements

Author contributions

Y.M., G.W., and T.C. conceived the study. G.W. designed the study. Z.S., Z.X., W.R., H.S., H.Z., Q.Y., A.X., and H.M. performed the experiments and data processing. Z.S., Z.X., and G.W. analyzed the data. G.W., T.C., and Y.M. supervised the project. G.W., Z.S., and Z.X. wrote the manuscript. All authors read, edited, and approved the final manuscript.

Competing interests

Z.S., Z.X., H.S., H.Z., T.C., G.W., and Y.M. are inventors of patents (application numbers: CN115851850A, WO2023046007A1, and 202410878271.0) disclosing the synthetic microorganisms with optimized starch biosynthetic pathways and remodeled cell metabolism and morphology. The remaining authors declare no competing interests.

Additional information

Supplementary information The online version contains supplementary material available at https://doi.org/10.1038/s41467-025-58067-z.

Correspondence and requests for materials should be addressed to Tao Cai, Guokun Wang or Yanhe Ma.

Peer review information *Nature Communications* thanks Seung Hwan Lee and the other, anonymous, reviewer(s) for their contribution to the peer review of this work. A peer review file is available.

Reprints and permissions information is available at http://www.nature.com/reprints

Publisher's note Springer Nature remains neutral with regard to jurisdictional claims in published maps and institutional affiliations.